Asociación Argentina
de Mecánica Computacional

Mecánica Computacional Vol XXIX, págs. 5929-5939 (artículo completo)
Eduardo Dvorkin, Marcela Goldschmit, Mario Storti (Eds.)
Buenos Aires, Argentina, 15-18 Noviembre 2010

EFFECTS OF FORESHORTENING AND OVERSIZING OF FLOW DIVERTING STENTS FOR INTRACRANIAL ANEURYSMS

Fernando Mut[a], **Rainald Löhner**[a], **Christopher M. Putman**[b] **and Juan R. Cebral**[a]

[a]*Center for Computational Fluid Dynamics, George Mason University, Fairfax, Virginia 22030, USA fmut@gmu.edu, http://web.cos.gmu.edu/~fmut*

[b]*Interventional Neuroradiology, Inova Fairfax Hospital,Falls Church, Virginia 22040, USA christopher.putman@inova.com*

Keywords: Hemodynamics, Cerebral Aneurysms, Flow Diverting Stents, Deployment.

Abstract. Understanding the effects of flow diverting stents is important to evaluate and plan treatments, identify possible failure modes and limitations, and improve the design of flow diverting devices. The purpose of this work was to develop methods for precise deployment of flow diverting stent models into patient-specific vascular geometries reconstructed from three-dimensional (3D) anatomical images of brain aneurysms. The stent is modeled as a series of interconnected wire segments that is released inside the vascular model under the influence of angular and stretching forces that try to recover the reference (un-deformed) configuration and contact forces with the vascular wall that constrain the stent to the vessel interior. This methodology attempts to properly capture the foreshortening characteristics of these devices, which is extremely important because in the majority of treatments the stents are oversized in order to achieve a good wall apposition against the parent artery. The methodology was tested against theoretical results of a series of stents released into straight tubes of varying diameters. The results indicate that the numerical models were able to reproduce the stent foreshortening characteristics in these situations to within a 1% error. Subsequently, the hemodynamic effects of the geometric deformation of the stent cells due to the foreshortening of oversized stents were studied using the patient-specific geometry of a giant internal carotid artery aneurysm with a wide neck. The results show that for an oversized stent, i.e. when it is deployed in an artery of smaller diameter, the changes in the geometry of the stent cells have a significant impact on its flow diverting characteristics. Specifically, the stent cells widen allowing a larger inflow into the aneurysm, thus reducing its hemodynamic performance. In conclusion, these effects must be considered when designing new devices or conducting clinical studies of stent efficacy.

1 INTRODUCTION

Cerebral aneurysms are the most common source of hemorrhagic strokes (Stehbens 1972). A cerebral aneurysm that ruptures has an associated rate of fatality of 50%, with another 20% suffering significant morbidity (Linn, Rinkel et al. 1996; Tomasello, D'Avella et al. 1998; Winn, Jane et al. 2002; Kaminogo, Yonekura et al. 2003). This terrible burden can be reduced by the appropriate aneurysm treatment by either traditional surgical clipping or endovascular intra-aneurysmal occlusion. The treatment of intracranial aneurysms has gone through dramatic changes with the introduction of interventional techniques. Endosaccular coiling of aneurysms has been shown to be effective and has arguably replaced surgery for the treatment of most aneurysms (Molyneux, Kerr et al. 2002). However, coiling has significant limitations in achieving durable occlusion of many large and giant aneurysms because of a propensity for recanalization. For this reason flow diverting stents are increasingly been considered as a therapeutic alternative to surgical clipping and endovascular coiling, especially for large complex aneurysms with wide necks affecting a long segment of the parent artery (Lylyk, Ferrario et al. 2005; Lövbald, Yilmaz et al. 2006; Szikora, Berentei et al. 2006). Many aneurysms of this type were extremely difficult or impossible to treat before the development of flow diverting stents for intracranial use. While the objective of coiling is to fill the aneurysm sac with metal and create a stagnant flow environment which eventually thromboses, the aim of flow diverting stents is to create a stable hemodynamic environment favorable for thrombosis by reconstructing the parent artery and redirecting the flow away from the aneurysm (Lylyk, Miranda et al. 2009). Since the stents are placed in the parent vessel, they must be porous in order to avoid occlusion of small perforating arteries branching off the main artery and possibly causing ischemic strokes. On the other hand the hemodynamic performance of the stents and the outcome of the procedures depend on the local stent porosity and geometric characteristics (Lieber, Stancampiano et al. 1997). Thus, understanding the effects of flow diverting stents is important to evaluate and plan treatments, identify possible failure modes and limitations, and improve the design of flow diverting devices.

The purpose of this work was to develop and test methods for realistic deployment of flow diverting stent models into patient-specific vascular geometries of brain aneurysms for subsequent hemodynamic analysis. The methodology attempts to properly capture the foreshortening characteristics of these devices, which is extremely important because in the majority of treatments the stents are oversized in order to achieve a good wall apposition against the parent artery. This paper also investigates the effects of stent foreshortening on the hemodynamic performance of flow diverting stents.

2 METHODS

2.1 Vascular Modeling

Anatomical images of cerebral aneurysms and the connected arteries are obtained using 3D rotational angiography (3DRA) during conventional transfemoral catheterization of the cerebral blood vessels. Rotational acquisitions are obtained during a six seconds contrast injection for a total of 24 cc of contrast agent on a Philips Integris biplane unit (Philips Medical Systems, Best, The Netherlands). The projection images are reconstructed into 3D voxel data using standard proprietary software (Philips XtraVision). Patient-specific vascular models are constructed from the 3DRA images using seeded region growing segmentation to recover the arterial network topology followed by iso-surface deformable models to recover the vascular geometry (Yim, Boudewijn et al. 2003; Cebral, Castro et al. 2005). The models are then smoothed using a non-shrinking algorithm (Taubin 1995) and arterial branches are truncated perpendicularly to their axes. The geometrical models are then used to generate volumetric computational grids composed of tetrahedral elements using an advancing front method (Löhner 2001; Cebral, Castro et al. 2005). These meshes are generated with a minimum uniform resolution of 0.01 cm to 0.02 cm.

2.2 Stent Modeling

The deployment of stent models into subject-specific vascular geometries can be done in a variety of ways. The stent design can be edited and manipulated using computer aided design (CAD) tools to deform it and map it or place it within the vascular model (Kim, Levy et al. 2007), or a complete structural dynamics calculation can be carried out to simulate the stent release and deformation process (Mortier, Holzapfel et al. 2010). In the former case, the final deformation will depend on the operations performed by the user and it will likely not capture important effects such as stent foreshortening. In the latter case, the final stent geometry will be determined by the choice of material properties of the stent model. However, in a clinical procedure there are a number of other factors that will affect the final stent geometry. Such factors include the release speed, whether the intervening neuroradiologist pushes or pulls the catheter during the deployment, etc. These factors then make the geometry of the deployed stent quite difficult to predict. However, in order to study the hemodynamic performance of different stents, it suffices to specify a number of different stent deployment "scenarios". For example, by prescribing the final diameter of the deployed stent and studying the effects on the aneurysm hemodynamics. Thus, a different approach was adopted. The idea was to develop a simple and efficient stent deployment methodology that captures the most important geometric effects such as foreshortening and at the same time allows for easy control or specification of the stenting "scenario". Similar strategies have been previously described but they have not been tested for stent foreshortening effects or control of the stenting

"scenario" (Appanaboyina, Mut et al. 2008; Mut, Appanaboyina et al. 2008; Larrabide, Kim et al. 2010).

The current technique comprises the following components: a) deployment of a cylindrical surface to specify the stenting "scenario", b) stent generation, mapping and initialization, and c) stent relaxation or deformation.

The stent deployment technique starts by deploying a cylindrical surface into the parent vessel. This is achieved by first extracting the centerline of the parent vessel using an algorithm that computes the minimum-length path over the local maxima of the distance to wall field (Antiga, Ene-Iordache et al. Feb. 2003). A discrete structured cylindrical surface is then generated within the parent vessel, and along a cubic spline interpolation of the centerline points. This cylindrical surface is then released under the influence of internal smoothing forces and external contact forces that prevents the cylinder points from crossing the parent vessel. The internal smoothing forces are obtained by differentiation of the following energy functional (see Figure 1-left panel):

$$E = \sum \frac{1}{2} k_l (l_z - l_z^0)^2 + \frac{1}{2} k_l (l_c - l_c^0)^2 + \frac{1}{2} k_a (\alpha - \frac{\pi}{2})^2 + \frac{1}{2} k_a (\beta - \pi)^2 \quad (1)$$

where l_z and l_c represent the distances between two consecutive points in the longitudinal and circumferential directions respectively, and α and β represent the internal and external angles of the individual cells. The minimum of energy is achieved when the cylinder is in its reference configuration, i.e., a perfectly straight cylinder with $L=N_l*l_z$ and $\pi*D=N_c*l_c$, where L and D are the total length and diameter of the cylinder, and N_l and N_c are the number of subdivisions in the longitudinal and circumferential directions, respectively. Note that the final cylinder diameter, and therefore the final stent diameter, can be controlled by setting the reference parameter l_c. The classical Newtonian equations of motions are then integrated in time using the Newmark method (explicit, central difference) with artificial damping until convergence is reached. The output of this step is a cylindrical surface that fits most of the internal vessel geometry and do not exceed the maximum preset value for the diameter.

The next step in the stent deployment methodology is the selection of the stent design. Initially, the stent design is represented as a collection of interconnected points in a 2D plane. These points are then mapped into the deployed cylindrical surface, and into a reference cylindrical surface. The reference cylindrical surface is generated is accordance with stent reference geometrical parameters, i.e., stent reference length and diameter. The output of this step is the stent in the initial deployment configuration, and the stent in its reference configuration.

Finally, the stent design is released under the influence of internal smoothing forces and external constraining forces that prevent the stent points to leave the cylindrical surface. These constraining forces enforce the "scenario" configuration of

the deployed stent. The internal smoothing forces are obtained by differentiation of the following energy functional (see Figure 1-right panel):

$$E = \sum \frac{1}{2} k_l (l_w - l_w^0)^2 + \frac{1}{2} k_a (\theta - \theta^0)^2 \tag{2}$$

where l_w and θ represent the length of the wire segments and the angle between any two consecutive wire segments, respectively. The minimum of energy is achieved when the stent is in its reference configuration. This state is achieved if the initial deployed stent is released without the influence of the external constraining forces. As before, the classical Newtonian equations of motions are integrated in time using the Newmark method until convergence is reached. The output of this step is the stent in its final deployment configuration.

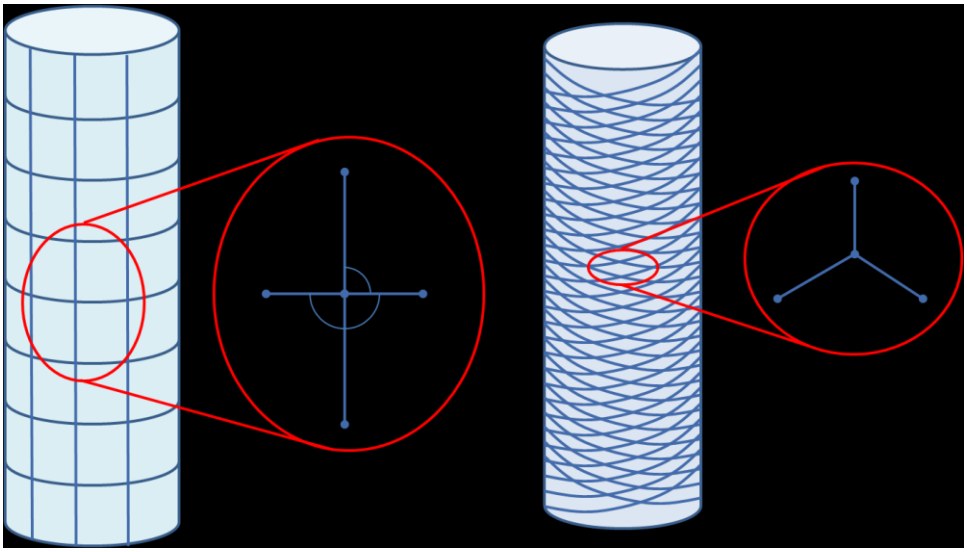

Figure 1: Angles and lengths definitions for the deployment of the cylinder (left) and stent design (right)

2.3 Blood Flow Modeling

Blood flows are mathematically modeled using the unsteady 3D Navier-Stokes equations for an incompressible Newtonian fluid with density ρ=1.0 g/cm^3 and viscosity μ=0.04 Poise. The governing equations are advanced in time using a fully implicit scheme that recasts the original equations as a steady-state problem in pseudo-time (ϑ) at each time-step (n):

$$u^{\xi}_{,\vartheta} + u^{\xi} \cdot \nabla u^{\xi} + \nabla p^{\xi} = \nabla \eta \, \nabla u^{\xi} - \frac{u^{\xi} - u^{n}}{\xi \, \Delta t} \tag{3}$$

$$\nabla \cdot u^{\theta} = 0 \tag{4}$$

where u is the velocity, p the pressure, η the kinematic viscosity, u^n denotes the velocity at the previous timestep and $u^{\xi}=(1-\xi)\, u^{n} + \xi \, u^{n+1}$. These equations are solved using a pressure-projection method where the spatial discretization is carried out using an edge-based upwind finite element method (Löhner 2001). The discretized

momentum equation is solved using a Generalized Minimal Residuals (GMRES) method and the discretized pressure Poisson equation is solved using an efficient deflated preconditioned conjugate gradients method (Mut, Aubry et al. 2009). Unstructured embedded grid methods are used to solve the governing equations for the models including endovascular devices, i.e. post-stenting models (Appanaboyina, Mut et al. 2008). For this purpose, the 3D stent wires are represented as a collection of overlapping spheres with diameters given by the wire thickness. These spheres are used to detect the grid edges intersected by the stent surface in order to adaptively refine the computational mesh and impose appropriate boundary conditions.

Physiologic flow conditions are derived from *in vivo* measurements of blood flows in normal subjects (Cebral, Castro et al. 2008). The waveforms measured in the cerebral arteries of normal volunteers are scaled with the area of the inlet boundary in order to achieve a mean wall shear stress of 15 dyne/cm^2 at the inlet. Fully developed velocity profiles are specified at the model inlet boundary using the Womersley solution (Taylor, Hughes et al. 1998). Traction-free boundary conditions are prescribed at the model outlets. Identical boundary conditions and model parameters are used in pre and post stenting models. The computational fluid dynamics (CFD) simulations are run for two cardiac cycles with a timestep of 0.01 sec. Results are presented for the second cycle.

3 RESULTS

3.1 Stent Release in Straight Tubes

The methodology was tested by releasing a stent in straight tubes of varying diameters. The stent had 32 wires, a diameter of 5.0 mm and a cell angle of 130^o (reference configuration). This stent was deployed into a series of straight circular tubes with diameters from 5.0 mm to 3.0 mm with a diameter increment of 0.25 mm. For each tube, a stent of smaller diameter is generated and released inside the tube. The stent then self-expands under the influence of the internal forces that try to recover the reference configuration and contact forces with the tube walls. Once the stent converges to an equilibrium configuration, its diameter, cell angle, and total length are measured and compared with corresponding analytic values. The analytic stent geometry is calculated under the assumption of perfectly incompressible wires and connections free to rotate. The results are presented in Table 1. This table lists the final values of stent diameter, cell angle and stent length after convergence, along with the analytic values and the corresponding relative errors. These results show that the stent deployment methodology is capable of accurately capturing the foreshortening characteristics of these devices. As can be observed in Table 1, the errors in the final stent diameter and length are below 1% and the error in the cell angle reaches a maximum of approximately 1.6%.

tube diameter (mm)	final diameter (mm)	diameter error	analytic angle (deg)	final angle (deg)	angle error	analytic length (mm)	final length (mm)	length error
5.00	5.0000	0.00%	130.00	130.00	0.00%	19.56	19.56	0.00%
4.75	4.7521	0.04%	118.86	119.79	0.79%	23.54	23.31	-1.01%
4.50	4.503	0.08%	109.31	110.57	1.15%	26.78	26.51	-0.99%
4.25	4.2546	0.11%	100.77	102.12	1.33%	29.51	29.29	-0.75%
4.00	4.0055	0.14%	92.95	94.27	1.43%	31.88	31.73	-0.46%
3.75	3.7561	0.16%	85.65	86.92	1.49%	33.95	33.87	-0.23%
3.50	3.5069	0.20%	78.75	79.97	1.54%	35.78	35.79	0.03%
3.25	3.2571	0.22%	72.19	73.33	1.58%	37.40	37.46	0.16%
3.00	3.0076	0.25%	65.88	66.93	1.59%	38.85	38.98	0.35%

Table 1: Release of a 5 mm diameter stent into tubes of varying diameters.

Figure 2 shows as an example the release of a 5.0 mm stent into a 4.0 mm tube. The left panel of this figure shows the reference (magenta) and final (yellow) stent geometries. The right panel shows the convergence history of the cell angle. These curves show the evolution of the minimum, maximum and average cell angle during the self expansion of the stent until it converges to the final configuration.

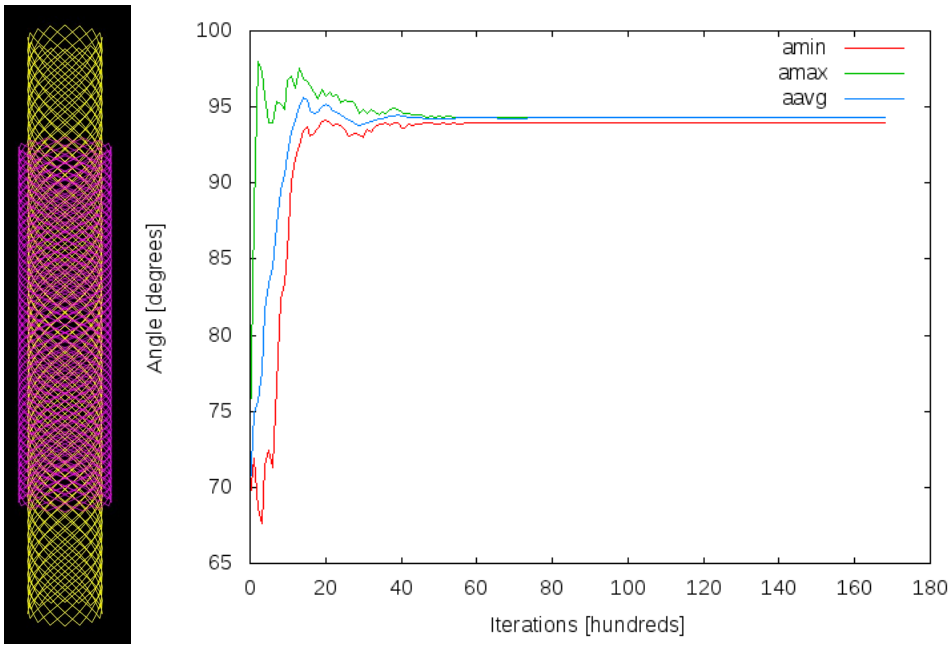

Figure 2: Deployment of a 5 mm stent into a 4 mm tube. Left: reference stent geometry (magenta) and after deployment (yellow). Right: minimum, maximum and average cell angle convergence history.

3.2 Effects of Stent Foreshortening

The effects of foreshortening on the hemodynamic performance of flow diverting stents were investigated using a patient-specific cerebral aneurysm geometry. The vascular geometry was reconstructed from a 3D rotational angiogram of a giant

aneurysm (26 mm) affecting a segment of the internal carotid artery. At the aneurysm location, the parent artery had a diameter of 3.5 mm. Three stents of 3.5 mm, 4.0 mm and 4.5 mm diameters were deployed and the corresponding intra-aneurysmal flow patterns were obtained. All simulations were carried out using the same pulsatile flow conditions. Visualizations of the inflow stream and aneurysm flow patterns at peak systole are presented in Figure 3. These visualizations show that as the stent is oversized (diameter increases) the reduction of the inflow stream decreases, i.e. more inflow into the aneurysm, and the flow pattern is less affected, i.e. it remains more disorganized and with higher velocities.

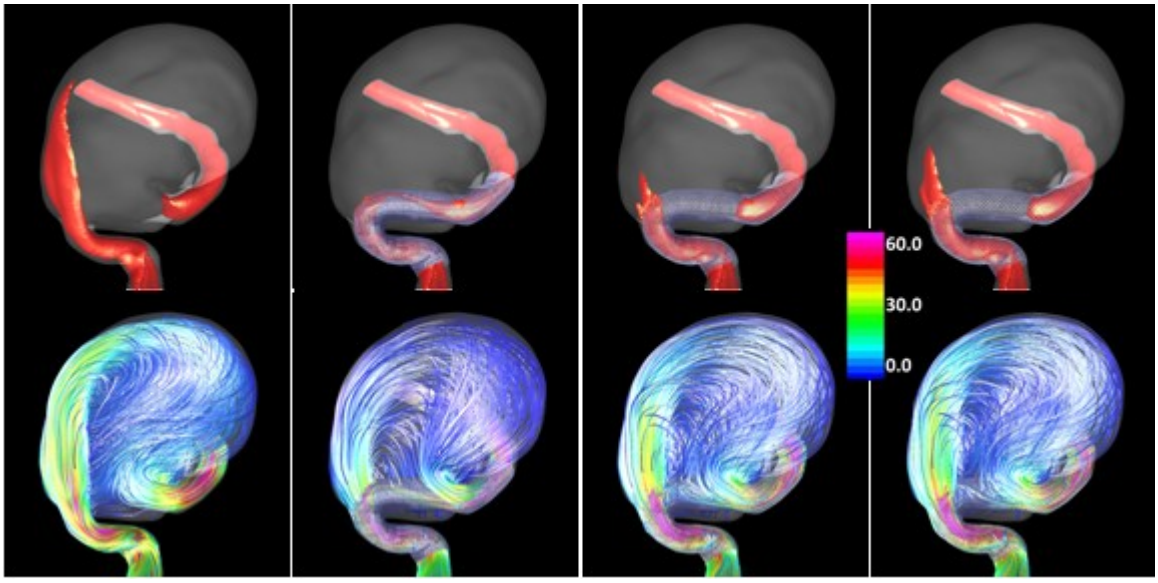

Figure 3: Peak systole flow pattern before and after deployment of stents of different diameter in a wide neck giant carotid artery aneurysm. Left to right: no stent, 3.5 mm stent, 4.0 mm stent, and 4.5 mm stent. Top row: iso-velocity surfaces (v=40 cm/s), bottom row: instantaneous streamlines.

The modifications of a number of hemodynamic quantities after deployment of the different stents are presented in Table 2. This table lists the values of the percent aneurysmal inflow with respect to the parent artery flow rate (Q_i), the total aneurysmal kinetic energy (K_e) and the maximum aneurysmal wall shear stress (MWSS). These variables were computed by first subdividing the computational model into vessel and aneurysm regions and generating a surface through the aneurysm orifice. Then, different variables are computed by taking integrals over the aneurysm volume (K_e), aneurysm surface (MWSS), and orifice surface (Q_i). The numbers listed in Table 2 correspond to the peak systole values, and the numbers in parenthesis represent the change in these variables from the pre-stenting configuration. These results indicate that because of the foreshortening characteristics of the stents, using oversized stents will result in decreased flow divertion and therefore a worse hemodynamic performance of the device, especially for this type of aneurysms with wide necks located near high vessel curvatures. These effects must be taken into account when designing new devices or when planning

endovascular interventions using these devices.

variable	no stent	3.5 mm stent		4.0 mm stent		4.5 mm stent	
Q_i	132%	60 %	(-54.5%)	97 %	(-26.5%)	103%	(-21.5%)
K_e	36.0	3.04	(-91.5%)	12.9	(-64.1%)	16.2	(-54.9%)
MWSS	4.53	0.66	(-85.4%)	1.87	(-58.7%)	2.23	(-50.6%)

Table 2: Change in hemodynamic quantities after deployment of stents of varying diameters.

As shown previously in Table 1, when the difference between the stent and vessel diameters increases (when the stent is oversized), the cell angle decreases, transforming a rhomboidal cell into a more squared cell. This geometric change results in a higher local porosity and consequently less blocking of the inflow stream and diversion towards the parent artery. This explains why stent foreshortening results in a decreased hemodynamic performance of these devices.

4 CONCLUSIONS

A methodology for deployment of stent models into patient-specific geometries of cerebral arteries with aneurysms has been developed and tested. This methodology is capable of accurately capturing the foreshortening characteristics of flow diverting stents. This is an important property because the local stent porosity depends on the geometry of the stent cells after deployment, which is affected by the foreshortening characteristics of the particular stent design. The results show that for an oversized stent, i.e. when it is deployed in an artery of smaller diameter, the changes in the geometry of the stent cells have a significant impact on its flow diverting characteristics. Specifically, the stent cells widen allowing a larger inflow into the aneurysm, thus reducing its flow diversion characteristics, i.e. its hemodynamic performance. In conclusion, these effects must be considered when designing new devices or conducting clinical studies of stent efficacy.

ACKNOWLEDGEMENTS

We thank Boston Scientific and Philips Healthcare for financial support.

REFERENCES

Antiga, L., B. Ene-Iordache, et al. Centerline computation and geometric analysis of branching tubular surfaces with application to blood vessel modeling. *11th International Conference in Central Europe on Computer Graphics, Visualization and Computer Vision'2003*, Plzen, Czech Republic, Feb. 2003.

Appanaboyina, S., F. Mut, et al. Computational Fluid Dynamics of Stented Intracranial Aneurysms using Adaptive Embedded Unstructured Grids. *International Journal for Numerical Methods in Fluids*, 57: 457-493, 2008.

Cebral, J. R., M. A. Castro, et al. Efficient pipeline for image-based patient-specific

analysis of cerebral aneurysm hemodynamics: Technique and sensitivity. *IEEE Transactions in Medical Imaging*, 24(1): 457-467, 2005.

Cebral, J. R., M. A. Castro, et al. Flow-area relationship in internal carotid and vertebral arteries. *Physiol Meas*, 29: 585-594, 2008.

Kaminogo, M., M. Yonekura, et al. Incidence and outcome of multiple intracranial aneurysms in a defined population. *Stroke*, 34(1): 16-21, 2003.

Kim, M., E. I. Levy, et al. Quantification of hemodynamic changes induced by virtual placement of multiple stents across a wide-necked basilar trunk aneurysm. *Neurosurgery*, 61(6): 1305-12, 2007.

Larrabide, I., M. Kim, et al. Fast virtual deployment of self-expandable stents: Method and in vitro evaluation for intracranial aneurysmal stenting. *Med Image Anal*, DOI 10.1016/j.media.2010.04.009, 2010.

Lieber, B. B., A. P. Stancampiano, et al. Alteration of hemodynamics in aneurysm models by stenting: influence of stent porosity. *Annals of Biomedical Engineering*, 25(3): 460-469, 1997.

Linn, F. H., G. J. Rinkel, et al. Incidence of subarachnoid hemorrhage: role of region, year, and rate of computed Tomography: a meta-analysis. *Stroke*, 27(4): 625-629, 1996.

Löhner, R. *Applied CFD techniques*, John Wiley & Sons, 2001.

Lövbald, K. O., H. Yilmaz, et al. Intracranial aneurysm stenting: follow-up with MR angiography. *J Mag Res Imaging*, 24: 418-422, 2006.

Lylyk, P., A. Ferrario, et al. Buenos Aires experience with the Neuroform self-expanding stent for the treatment of intracranial aneurysms. *Journal of Neurosurgery*, 102(2): 235-241, 2005.

Lylyk, P., C. Miranda, et al. Curative endovascular reconstruction of cerebral aneurysms with the pipeline embolization device: the Buenos Aires experience. *Neurosurgery*, 64(4): 632-642, 2009.

Molyneux, A., R. Kerr, et al. International Subarachnoid Aneurysm Trial (ISAT) Collaborative Group. International Subarachnoid Aneurysm Trial (ISAT) of neurosurgical clipping versus endovascular coiling in 2143 patients with ruptured intracranial aneurysms: a randomised trial. *Lancet*, 360(9342): 1267-1274, 2002.

Mortier, P., G. A. Holzapfel, et al. A novel simulation strategy for stent insertion and deployment in curved coronary bifurcations: comparison of three drug-eluting stents. *Ann Biomed Eng*, 38(1): 88-99, 2010.

Mut, F., S. Appanaboyina, et al. Simulation of stent deployment in patient-specific cerebral aneurysm models for their hemodynamics analysis. *ASME Summer Bioengineering Conference*, Marco Island, Florida, 2008.

Mut, F., R. Aubry, et al. Fast numerical solutions in patient-specific simulations of arterial models. *Comm Num Meth Eng*, DOI 10.1002/cnm.1235, 2009.

Stehbens, W. E. Intracranial aneurysms. *Pathology of the Cerebral Blood Vessels*. St. Louis, Misoury, CV Mosby**:** 351-470, 1972.

Szikora, I., Z. Berentei, et al. Endovascular treatment of intracranial aneurysms with

parent vessel reconstruction using balloon and self expandable stents. *Acta Neurichirurgica*, 148: 711-723, 2006.

Taubin, G. A signal processing approach to fair surface design. *Proc. 22nd Annual Conference on Computer Graphics and Interactive Techniques (SIGGRAPH 1995)*, Los Angeles, CA, 1995.

Taylor, C. A., T. J. R. Hughes, et al. Finite element modeling of blood flow in arteries. *Computer Methods in Applied Mechanics and Engineering*, 158: 155-196, 1998.

Tomasello, F., D. D'Avella, et al. Asymptomatic aneurysms. Literature meta-analysis and indications for treatment. *Journal of Neurosurgical Science*, 42(1): 47-51, 1998.

Winn, H. R., J. A. Jane, et al. Prevalence of asymptomatic incidental aneurysms: review of 4568 arteriograms. *Journal of Neurosurgery*, 96(1): 43-49, 2002.

Yim, P. J., G. Boudewijn, et al. Isosurfaces as deformable models for magnetic resonance angiography. *IEEE Trans on Medical Imaging*, 22(7): 875-881, 2003.